Resonant Structure in Near-Threshold Electron Excitation of Krypton

N. Swanson, J. W. Cooper, and C. E. Kuyatt
National Bureau of Standards, Washington, D. C. 20234
(Received 1 May 1973)

By using a monochromator-analyzer combination, electron-excitation functions of the lowest-lying electronic states of krypton have been obtained at a scattering angle of 45° in the near-threshold region (9–14 eV). All excitation functions display a complex resonant structure. Additional data have been obtained on elastic scattering at 45° to provide further information on the resonances. In addition to the $4p^5 5s^2$ $J = 3/2, 1/2$ resonance doublet, a number of narrow resonances appear below about 12 eV in both the excitation data and elastic scattering which correlate in energy with recent measurements on transmission by Sanche and Schulz. Broad resonant structure is found in a number of the excitation curves and the excitation process in the near-threshold region appears to be dominated by resonant effects. An analysis of the elastic-scattering data on the $4p^5 5s^2$ doublet is presented and resonance parameters obtained compared with theory. A comparison of the narrow resonant structure data with optical absorption data on Rb I obtained by Beutler indicates that the narrow resonances in the 10.5–12-eV region are probably due to levels of the $4p^5 5s 4d$ configuration.

I. INTRODUCTION

Near-threshold excitation of the lower excited states of atoms by electron impact is expected to exhibit a complex resonance structure owing to the formation of temporary negative-ion states (resonances).[1] Within a few electron volts of any excitation threshold, the excitation cross section is expected to be dominated by resonant effects. During the past several years the effects of resonances on the excitation cross sections for the first few excited states of H and He have been the subject of a number of experimental[2–5] and theoretical studies.[6–8] Experimental studies for other atomic systems have been limited to transmission measurements,[9,10] elastic-scattering,[11] electron trapping[12] or scavenging techniques,[13] and observations of fluorescence radiation produced by monoenergetic electron beams.[14] These studies have demonstrated that resonant effects are present in all of the rare gases, Hg, and Na, but have not provided detailed information on the effects of resonances on individual states of excitation.

The present study deals with the resonant effects on the excitation functions for the lower excited states of krypton which belong to the $4p^5 5s$ and $4p^5 5p$ configurations. The main method used is a measurement of the energy dependence of inelastic scattering at an angle of 45° using a monochromator-analyzer combination described in detail below. Even though the instrument used is capable of moderately high resolution (~20–100 meV) only 6 of the 14 levels belonging to the $4p^5 5s$ and $4p^5 5p$ configurations of krypton could be resolved from each other or from neighboring levels of the $4p^5 4d$ configuration. Excitation data corresponding to unresolved levels was taken in order to obtain information on the effects of the resonant structure on the excitation functions. The data on excitation were supplemented by measurements of the resonant structure in elastic scattering at 45° using the same apparatus.

Even though the measurements reported here are limited to a scattering angle of 45°, some general features are immediately apparent from the data and from a comparison with previous measurements. A number of sharp resonances have recently been reported[10] in transmission measurements. Several of these resonances appear at the same energies in our elastic-scattering data and in some, but not all, of the excitation functions reported here. As in the case of helium[4,5] the excitation function immediately above threshold generally shows both broad and sharp resonant structure and is often smaller several electron volts above threshold than in the near-threshold region.

The data presently available are not sufficient to provide a detailed theoretical analysis of the resonant structure. However, some comparisons with theory and other experiments can be made. The two lowest resonances in krypton have been described as a doublet with the configuration $4p^5_{3/2,1/2} 5s^2$.[15] This designation is supported by extracting shape parameters from the 45° elastic-scattering data and comparing these with theoretical parameters obtained from a phase-shift analysis of the scattering at 45°.

Classification of the resonant structure lying above the excitation threshold is more difficult. However, a comparison of the available data with optical transmission measurements made on Rb I (which is isoelectronic with Kr^-) indicates that the sharp resonance features lying immediately above

the excitation threshold probably are due to levels of the $4p^5 5s4d$ configuration.

The outline of the remainder of this paper is as follows. Section II is devoted to a description of the apparatus and to the method of data collection. Section III contains the results of our elastic scattering data and the theoretical analysis of the $4p^5_{3/2,1/2}5s^2$ doublet resonances.

The results of the excitation measurements are presented and described in Sec. IV. Section V is devoted to an analysis of the resonant structure lying above the excitation threshold and Sec. VI presents a summary and conclusions.

II. APPARATUS

The instrument used for these measurements was an electron monochromator-analyzer combination contained inside a 13-in.-i.d. cylindrical stainless-steel vacuum chamber as shown in Fig. 1. The static gas-target cell was hollowed out from $\frac{1}{2}$-in.-diam molybdenum rod, with a 0.065-in.-diam entrance aperture and 0.025-in.-diam exit apertures at $\theta = 0°$, 30°, 45°, and 90°. The krypton pressure inside the gas cell was about 20 mTorr and about 1000 times less than that in the surrounding vacuum chamber. The vacuum chamber was pumped by a 9-in.-diam mercury diffusion pump in series with a high-conductance liquid-nitrogen trap and a freon baffle. The entire chamber is bakeable to about 325°C.

The electron monochromator section uses a Pierce-type gun with an indirectly heated Philips type A cathode. The energy dispersing element is a pair of concentric copper hemispheres of mean radius 2 in., with a $\frac{1}{2}$-in. gap between them. The entire monochromator section can be rotated about the scattering center in fixed angular steps of 5 deg. from 0° to 100°. The scattering angle is not adjustable from outside the vacuum chamber, however, so a given series of runs can be made at only one scattering angle.

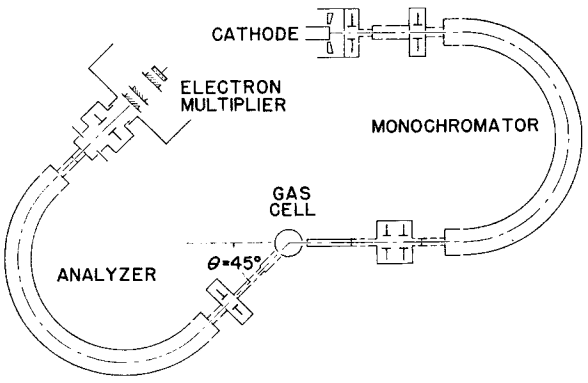

FIG. 1. Diagram of the electron spectrometer, with positions of deflection plates and apertures indicated.

The analyzer section focuses the scattered electrons at the entrance of the analyzer spheres (identical to the monochromator spheres). The energy-analyzed electrons are then focused and accelerated into an electron multiplier. The electron multiplier has 18 Be-Cu dynodes, with a gain of about 5×10^6 at 190 V/dynode in typical operation. The multiplier anode is connected to a 50-Ω impedance line at the multiplier housing, and the output pulses produced by the individual scattered electrons are amplified by a fast amplifier chain, with a typical output pulse half-width of approximately 15 nsec. A discriminator is used to remove lower-amplitude noise pulses, and the resultant pulses are either counted on a scaler and stored in an on-line computer, or displayed on a count rate meter connected to an X-Y recorder. The on-line computer can also control a digital power supply, and the instrument has been operated with computer-controlled sweeps of either incident electron energy or energy loss. The scaler counts for a selected time interval at each energy increment, and the resultant count is stored in memory. Repetitive scans can be made automatically under computer control and are desirable since this mode of operation tends to average background noise. Counting times of 17 msec per step are used with the present system to reduce 60-Hz noise.

All electron lens elements are made of copper, and the beam defining apertures are made from 0.005-in.-thick molybdenum. The remaining support pieces and vacuum housing are made from type 304 stainless steel.

The instrument is designed to operate at electron energies in the target gas cell of 5–50 eV. Typical operation at nonzero scattering angles is 25–100-meV full width at half-maximum (FWHM) at an incident energy of 10 eV.

To eliminate the production or scattering of low-energy electrons from apertures at the entrance and exit of the energy-selecting hemispheres and the target gas cell, real beam-defining apertures are located in lens elements at high potential, and imaged onto the entrance and exit planes of the hemispheres and gas cell at low potential. Thus low-energy electrons formed by edge scattering on the entrance sides of these elements are retarded out of the beam. Similarly, on the exit sides of these elements, electrons are accelerated to higher energies before passing through an energy- or beam-defining aperture. The apertures in the gas cell control the gas efflux and do not define the beam size.

Two pairs of rectangular coils are used to null the earth's field to within 5 mG at the target gas

cell, with residual dc fields in other parts of the chamber less than 20 mG. All electrical leads except those for the electron multiplier are rf bypassed at the vacuum feedthrough.

The data presented here were taken over approximately a 1-yr period during which major improvements were made in the apparatus. Thus, part of the data (the $4p^5 5s$ excitation curves of Figs. 4 and 5) were obtained from X-Y recorder traces with background subtracted graphically, whereas the rest of the data were obtained from computer-controlled sweeps. At least two sweeps of all curves shown were taken, and attempts have been made to remove features of the data which appeared to be spurious.

As pointed out by Schulz,[1] excitation data obtained in this type of apparatus are degraded in the region a few tenths of an eV above threshold due to the fact that the analyzer must accept low-energy electrons without energy discrimination or chromatic aberration. Some of the excitation curves presented show sharp peaks in the region immediately above threshold, whereas others do not. The above-mentioned effects have been accounted for to some extent by obtaining background traces with the instrument tuned to accept electrons with energies corresponding to excitation well away (0.1 or 0.2 eV) from any known excited state. All of the peaks immediately above threshold reported here appear to be real but their relative magnitude is more uncertain than features lying at higher energies above threshold.

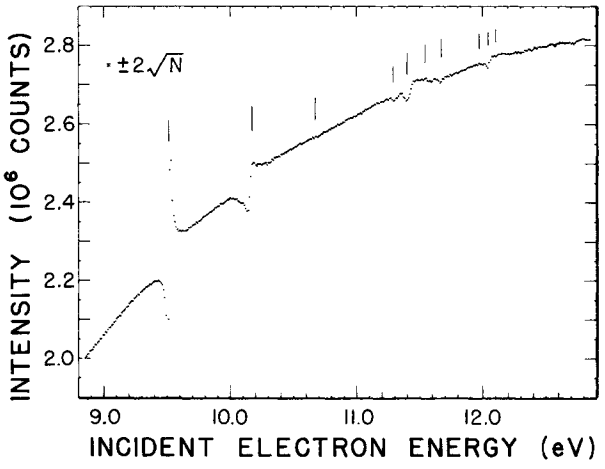

FIG. 2. Resonances observed in elastic scattering in Kr at 45° based on 2800 computer-controlled sweeps with 10-meV steps and a dwell time of 17 msec. The instrumental resolution was ≈40 meV. The energy scale was set by assuming the center of the lowest resonance to be at 9.515 eV. Vertical lines indicate the positions of features observed in transmission (Ref. 10). The "error bar" $\pm 2\sqrt{N}$, where N is the number of counts/channel indicates the statistical accuracy of the data.

III. RESONANCES IN ELASTIC SCATTERING

A. $4p^5_{3/2,1/2}5s^2$ Doublet

Resonances lying at 9.47 and 10.10 have previously been observed in transmission.[15] These resonances were recently observed in a differential-transmission measurement by Sanche and Schulz[10] who, after a careful calibration of their energy scale, place the centers of the resonances at (9.515 and 10.175 eV) ± 30 meV, respectively. These resonances as observed in elastic scattering at 45° are shown in Fig. 2. The energy scale has been set by taking the center of the first resonance to be 9.515 eV. This places the center of the higher-energy resonance at ≈ 10.155 eV, somewhat lower than that observed by Sanche and Schulz.

The lower-energy resonance appears as an asymmetric line profile similar to that observed at 40° for the analogous resonance in electron-argon scattering by Andrick and Ehrhardt.[16] The higher-energy resonance is broader, has approximately the same shape, and is smaller in amplitude.

The scattering in the vicinity of the resonances can be analyzed in terms of the phase shifts for elastic scattering. Since the spin-orbit splitting between the two resonances is large compared to their apparent width it is a good approximation to consider them as isolated resonances. However, a spin-dependent analysis is necessary.

The differential scattering cross section at angle θ can be expressed as[17]

$$I(\theta) = |f|^2 + |g|^2, \tag{1}$$

where

$$f(\theta) = (2ik)^{-1} \sum_l \{(l+1)[\exp(2i\delta_{l+1/2}) - 1] + l[\exp(2i\delta_{l-1/2}) - 1]\} P_l(\cos\theta), \tag{2a}$$

$$g(\theta) = (2ik)^{-1} \sum_l [\exp(2i\delta_{l+1/2}) - \exp(2i\delta_{l-1/2})] P_l^1(\cos\theta), \tag{2b}$$

$\delta_{l\pm1/2}$ are the phase shifts corresponding to scattering for a given l value and alternative spin states, and P_l, P_l^1 are Legendre functions. The various terms appearing in Eq. (2) will be labeled $^2S_{1/2}$, $^2P_{3/2}$, $^2P_{1/2}$, $^2D_{5/2}$, $^2D_{3/2}$, etc., corresponding to $j = l \pm \frac{1}{2}$ for various l values. An isolated resonance in elastic scattering will correspond to one of the phase shifts $\delta_{l\pm1/2}$ increasing by π in a narrow energy range while all other terms remain constant. Accordingly we can separate Eqs. (2a) and (2b) as follows:

$$f(\theta)=(2ik)^{-1}\Big(\sum_{\substack{j\neq\bar{j}\\ l}}\{(l+1)[\exp(2i\delta_{l+1/2})-1]+l[\exp(2i\delta_{l-1/2})-1]\}P_l(\cos\theta)$$
$$-P_{\bar{l}}(\cos\theta)+(\bar{j}+\tfrac{1}{2})\exp(2i\delta_{\bar{j}})P_{\bar{l}}(\cos\theta)\Big)\,, \tag{3a}$$

$$g(\theta)=(2ik)^{-1}\Big(\sum_{\substack{j\neq\bar{j}\\ l}}[\exp(2i\delta_{l+1/2})-\exp(2i\delta_{l-1/2})]P_l^1(\cos\theta)+(\bar{j}-\bar{l})\exp(2i\delta_{\bar{j}})P_{\bar{l}}^1(\cos\theta)\Big)\,, \tag{3b}$$

where $\delta_{\bar{j}}$ is the resonant phase shift corresponding to $\bar{j}$ and $\bar{l}=\bar{j}\pm\frac{1}{2}$.

The phase shifts $\delta_{l\pm1/2}$ will, in general, differ due to spin-orbit interaction, but the differences are expected to be small for krypton. Under this assumption, $g(\theta)$ vanishes except in the vicinity of a resonance.

The resonant terms can be expressed as

$$f^R(\theta)=(2ik)^{-1}(\bar{j}+\tfrac{1}{2})\exp[2i(\bar{\delta}_{\bar{j}}-\cot^{-1}\epsilon)]P_{\bar{l}}(\cos\theta)\,, \tag{4a}$$

$$g^R(\theta)=(2ik)^{-1}(\bar{j}-\bar{l})\exp[2i(\bar{\delta}_{\bar{j}}-\cot^{-1}\epsilon)]P_{\bar{l}}^1(\cos\theta)\,, \tag{4b}$$

where $-\cot\epsilon=(E-E_0)/\frac{1}{2}\Gamma$ describes the variation of $\delta_{\bar{j}}$ as it increases by π going through a resonance of width Γ at energy $E-E_0$ and $\bar{\delta}_{\bar{j}}$ is the nonresonant phase shift. The nonresonant parts of $f(\theta)$ and $g(\theta)$ reduce to

$$f^{\rm NR}(\theta)=(2ik)^{-1}\Big(\sum_{l\neq\bar{l}}[(2l+1)\exp(2i\bar{\delta}_l)-1]P_l(\cos\theta)+\{(2\bar{l}-\bar{j})[\exp(2i\bar{\delta}_{\bar{l}})-1]-\bar{j}\}P_{\bar{l}}(\cos\theta)\Big)\,, \tag{5a}$$

$$g^{\rm NR}(\theta)=(2ik)^{-1}(\bar{l}-\bar{j})\exp(2i\bar{\delta}_{\bar{j}})P_{\bar{l}}^1(\cos\theta)\,. \tag{5b}$$

The variation of the scattering amplitudes is best illustrated by an Argand diagram as shown in Fig. 3 for resonances corresponding to the $\frac{3}{2}$, $\frac{1}{2}$ doublet resonances in krypton at 45°. The diagram was drawn using the phase shifts calculated by Holtzmark[18] interpolated at an energy of 9.5 eV. The phase shifts used are given in Table I.

Figure 3 illustrates graphically the terms making up $f(\theta)$ and $g(\theta)$ including l values through $l=3$.

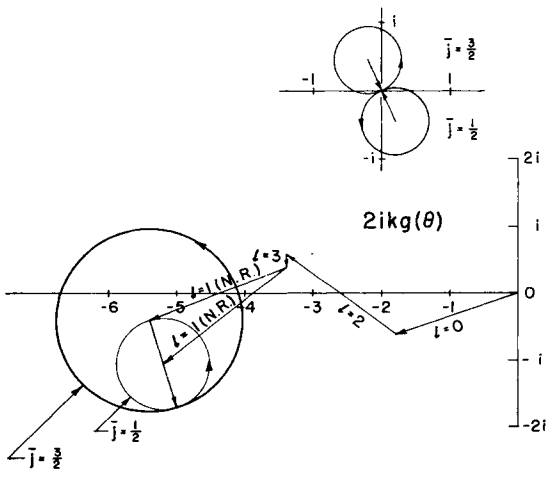

FIG. 3. Argand diagrams showing the resonant and nonresonant contributions to the scattering amplitudes for the $4p^5_{3/2,1/2}5s^2$ resonances.

$f(\theta)$ is composed of nonresonant parts corresponding to $l=0$, 2, and 3 and a resonant and nonresonant part corresponding to $\bar{l}=\bar{j}\pm\frac{1}{2}$, which is different for each resonance. The resonant terms lie on the same vector and have amplitude ratios 2 to 1. The diagram indicates that $f(\theta)$ should decrease in amplitude and then increase as the resonance vector moves in a counterclockwise direction for each resonance.

The $g(\theta)$ term is zero off resonance and rises to a maximum value at $\cot^{-1}\epsilon=\frac{1}{2}\pi$, the resonance position, for both $\bar{j}=\frac{3}{2}$ and $\frac{1}{2}$ resonances.

The resonance cross section is obtained by adding the squares of the scattering amplitudes $|f(\theta)|^2$ and $|g(\theta)|^2$. The sum of these two components can be cast in the resonant form[19]

$$I(\theta)=\sigma_b+\sigma_a(q+\epsilon)^2/(1+\epsilon^2) \tag{6}$$

as shown in Appendix A.

Resonant parameters q and $\rho=[\sigma_a/(\sigma_a+\sigma_b)]^{1/2}$

TABLE I. Resonance parameters for the $4p^5_{3/2,1/2}5s^2$ resonances. The theoretical values (in parentheses) are based on the following phase shifts (Ref. 18) estimated at 9.5 eV: $\delta_0=-71°$, $\delta_1=-40°$, $\delta_2=53°$, $\delta_3=5°$.

E_0	Resonance	q	Γ	ρ	Assumed resolution (meV)
9.515	$\frac{3}{2}$	1.13 (1.05)	0.0038	0.58 (0.72)	40
9.515		1.05	0.0047	0.57	40
9.515		1.07	0.0060	0.48	20
10.137	$\frac{1}{2}$	0.42 (1.10)	0.073	0.20 (0.46)	40
10.150		0.64	0.035	0.20	20

for each resonance may be obtained from the previous analysis. In order to provide a comparison with the experimental data, the resonance parameters for the $^2P_{3/2}$ and $^2P_{1/2}$ profiles shown in Fig. 2 were determined from the observed data. The procedure adopted was to assume the true cross section was of the form of Eq. (6) and that the energy spread of the electron beam was Gaussian. The background cross section was approximated by a quadratic function, and the calculation was performed by obtaining a least-squares fit of the parameters ρ, E_0, Γ, q, and the two leading terms of the background to the observed data.[20] The procedure was carried out twice for the $^2P_{3/2}$ resonance assuming energy spreads of 0.04 eV (the measured FWHM) and once assuming a spread of 0.02 eV in order to determine the effects of varying energy spreads and different sets of data on the parameters. The results along with the theoretical estimates are shown in Table I.

The values of q and ρ obtained from the $^2P_{3/2}$ resonance are in good agreement with those obtained from the phase-shift data. The theoretical value of ρ is larger and while a part of this discrepancy may be due to background in the experiment the major part is probably due to inaccuracies in the phase shifts. The width of the $^2P_{3/2}$ resonance is found to be much smaller than the resolution of the apparatus. Although the actual width is uncertain the true width is probably less than the 6 meV obtained using 20-meV resolution.

The agreement between calculated and observed resonance parameters is much poorer for the $^2P_{1/2}$ resonance. This is not surprising since the fact that this resonance lies above two levels of the $4p^5_{3/2}5s$ configuration means that the analysis in terms of phase shifts would only be applicable if decay into the excited states were negligible. The low values of q and ρ obtained from the data and the large width indicate that an appreciable fraction of the decay of this resonance is to the excited state, in agreement with observation.

B. Resonances in the 10.5-12.10-eV Region

Sanche and Schulz[10] have reported sharp features in transmission at 10.69, 11.29, 11.40, 11.54, 11.67, 11.97, 12.04, and 12.10 eV. These features correspond to maxima or minima in the derivative of the transmitted current. The energy positions of these features are also shown on the 45° elastic-scattering curve of Fig. 2. Resonant structure is apparent in the elastic scattering results at ≈11.30, ≈11.42, and ≈12.04 eV. The general shape of the two strongest features (≈11.42 and ≈12.04 eV) appears to be similar to that of the $4p^5_{1/2}5s^2\,^2P_{1/2}$ resonance, whereas the resonances at ≈11.30 and ≈11.67 appear as minima in the elastic data.

No sharp variations are evident in the elastic-scattering results at 10.69, 11.54, 11.97, and 12.10 eV. However, these features appear to be much weaker than the others in the results reported in Ref. 10. The elastic-scattering results also appear to show a broad but weak enhancement between 11.45 and 11.60 eV and a similar feature between 12.05 and 12.20 eV.

IV. EXCITATION FUNCTIONS

An energy-level diagram of krypton is shown in Fig. 4. The figure has been drawn to illustrate the following points: (i) The four levels of the $4p^5_{3/2,1/2}5s$ configurations are well separated in energy; (ii) the $4p^5_{3/2}5p$ levels separate into four groups; however, only two levels are separated from the rest by more than 35 meV, a rough criterion for being able to resolve them using the present apparatus; (iii) above 12 eV it is impossible to resolve any single level with ≈35-meV resolution.

The energy-level structure thus limits the study of excitation functions to the $4p^5_{3/2,1/2}5s$ configuration and two levels of the $4p^5_{3/2}5p$ configuration within the current resolution. Excitation functions

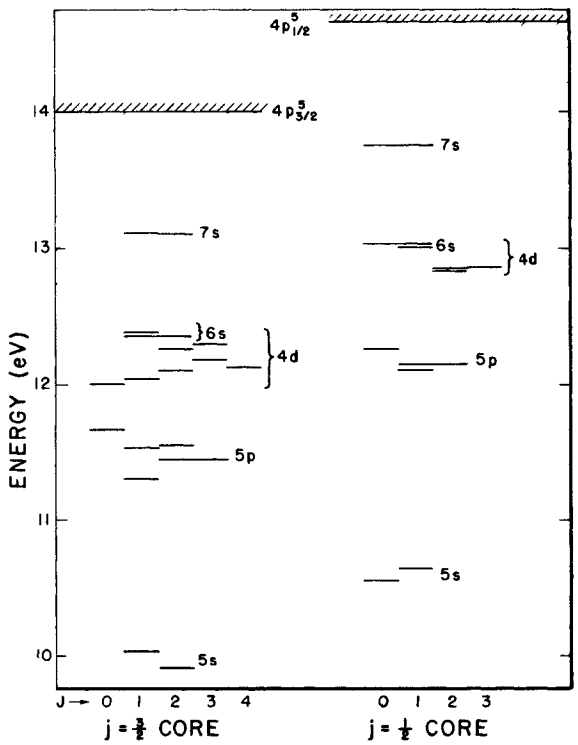

FIG. 4. Energy-level diagram for krypton. Only levels with 5s, 6s, 7s, 5p, and 4d electrons are indicated. Above ≈12.75 eV the level structure becomes dense due to states with higher quantum numbers as indicated by the shading.

for other levels will correspond to unresolved excitation of two or more levels.

A. $4p^5_{3/2}5s$ Excitation

Excitation curves for the four $4p^5_{3/2,1/2}5s$ levels are shown in Figs. 5 and 6. Each curve has been obtained by subtracting curves obtained at the indicated energy loss and at a somewhat higher energy loss (100–200 meV), which gives the background of scattered electrons. A typical background trace is also shown in Fig. 5. The energy scales have been set by estimating where the onset of excitation occurs in each case and are correct to about ± 0.03 eV.

The $4p^5_{3/2}5s$ excitation curves shown in Fig. 5 show a number of features that correlate with the sharp resonances that occur in elastic scattering and transmission. Sharp features are present in the $J=2$ level (9.91-eV excitation energy) at 10.14, 11.29, 11.42, 11.66, and 12.04 eV and corresponding features are also present in the excitation function for the $J=1$ level (10.03-eV excitation energy). The most prominent feature in either spectrum is the large peak at 10.14 eV corresponding to decay of the $4p^5_{1/2}5s^2\,{}^2P_{1/2}$ resonance into the $J=1$ $4p^5_{3/2}5s$ level. Note that there is little decay of this resonance into the $J=2$ $4p^5_{3/2}5s$ level. Since this resonance can only decay by an Auger-like process (the angular momentum of the $4p^5$ core must change during the decay process), the emisson of electrons with $l=2$ is highly unlikely, i.e., in the possible decay processes

$$4p^5_{1/2}5s^2 \rightarrow 4p^5_{3/2}5s(J=1,2)\epsilon d \qquad (6a)$$

$$\rightarrow 4p^5_{3/2}5s(J=1)\epsilon s\,; \qquad (6b)$$

only (6b) occurs with appreciable probability.[21]

There is a shoulder on the threshold side of the 10.14-eV resonance indicating that the resonance is further above threshold (0.11 eV) than the resonance width (FWHM = 0.06 eV).

The $4p^5 5s$ $J=2$ excitation function shows some evidence of decay of the $4p^5_{1/2}5s^2\,{}^2P_{1/2}$ resonance at 10.14 eV but an additional feature appears at 10.04 eV. We interpret this as a cusp effect caused by the opening up of the channel for $4p^5_{3/2}5s$ $J=1$ excitation.[22]

In addition to the sharp features present in $4p^5_{3/2}5s$ excitation broad features appear at approximately 11.1 eV in both curves and at ≈12 eV for $J=1$ excitation.

Resonant structure similar to that in $4p^5_{3/2}5s$ excitation also appears in the $4p^5_{1/2}5s$ $J=0$ (10.56-eV excitation energy) and $J=1$ (10.64-eV excitation energy) curves in Fig. 6. Sharp features are present at the thresholds and at 11.29, 11.42, and in the region between 12.0 and 12.2 eV. A broad peak is present at ≈11.7 eV in the $J=1$ excitation curve but is much smaller if at all present in $J=0$ excitation. The average cross section for $J=0$ excitation is much smaller than for any of the other $4p^5 5s$ levels. The peak at threshold in $J=0$ excitation is somewhat uncertain since a large part of the peak is due to background as shown in Fig. 5.

B. $4p^5_{3/2}5p$ Excitation

Excitation functions corresponding to $4p^5_{3/2}5p$ levels are shown in Fig. 7. Only the states $J=1$

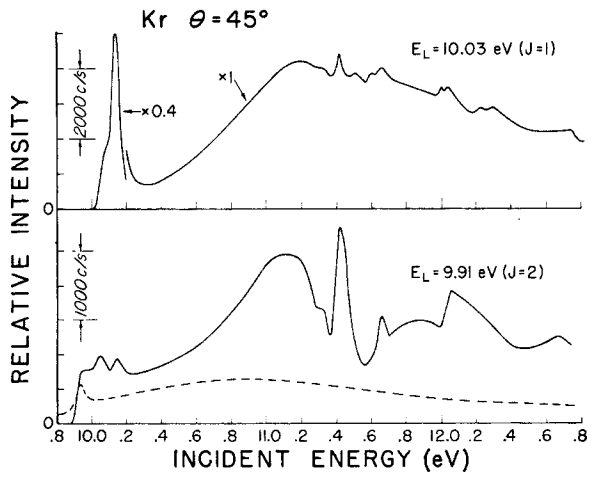

FIG. 5. Excitation functions of the $4p_{3/2}5s$ states of Kr, measured with an instrumental resolution ≈50 meV. The background, shown in the lower figure as a dashed line, has been subtracted from the original x-y recorder traces to give the solid curves.

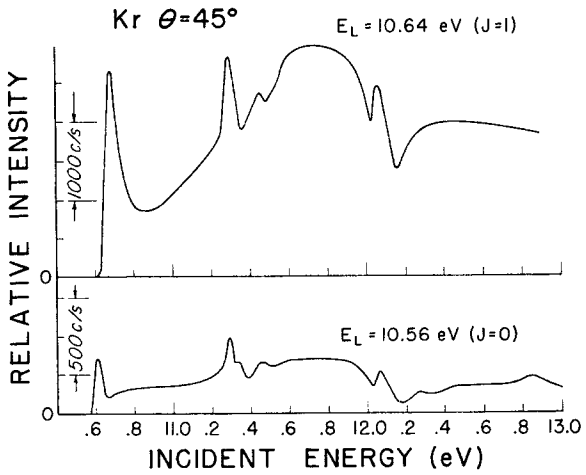

FIG. 6. Excitation functions of the $4p^5_{1/2}5s$ states of Kr, measured with an instrumental resolution ≈50 meV. The background has been subtracted as in Fig. 5.

(11.303-eV excitation energy) and $J=0$ (11.666 eV) are resolved in these spectra. The other curves represent both $J=2$ and 3 levels (at 11.444 eV) and

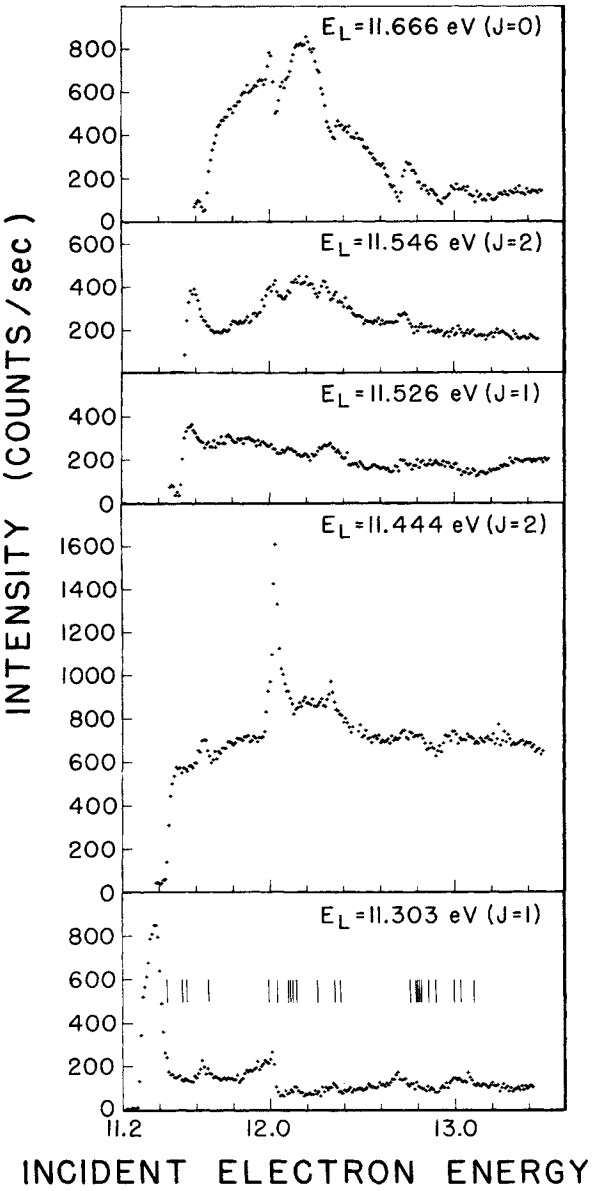

FIG. 7. Excitation functions of the $4p^5_{3/2}5p$ states of Kr, measured with an instrumental resolution ≈30 meV. The plots give the average counts/sec as a function of incident electron energy for five computer-controlled sweeps of the spectrum. Points were recorded every 10 meV with 1-sec/point dwell times. Again a smooth background intensity has been subtracted from the measured intensities to make the plots. To compare the intensities of this figure with those of Figs. 5 and 6 adjusted for equal resolution, the counts/sec of this figure should be multiplied by approximately 3. Energy levels corresponding to $J=0$, 1, 2 levels of $5p$ and $4d$ levels of Kr are shown in the figure.

$J=1$ and 2 levels (at 11.526 and 11.546 eV).

Sharp features appear in some or all of these curves at approximately 11.40, 11.64, 12–12.1, 12.35, 12.72, and 12.9 eV.

A number of sharp features appear in most of the curves which may be due to effects of opening of new channels of excitation. No definite correlation of these sharp features with excitation thresholds appears to be possible. However, energy levels of excited states are plotted on the curves. Strong features are apparent at 11.42 (11.303-eV excitation), 12.04 (11.444-eV excitation), and 12.00 and 12.8 eV (11.666-eV excitation), which appear to be due to the formation of negative ion resonant states.

The over-all shapes and relative intensities of the curves are quite different. The 11.303- and 11.526-eV excitation curves appear quite flat, whereas the others seem to show evidence of broad resonance structure in the region between threshold and 13 eV. This effect is especially clear in 11.666-eV excitation. Also, note the difference in shape of the 11.526- and 11.546-eV excitation curves even though the energy resolution of the two levels is not complete in this case.

V. INTERPRETATION OF LOW-LYING RESONANCES

The analysis[23] of the resonant structure in krypton is difficult due to the fact that intermediate coupling must be used to characterize the states of the $4p^5_{3/2,1/2}5s$ and $4p^5_{3/2}5p$ configurations and also because it is uncertain whether or not quartet virtual negative ion states may be formed due to spin-orbit coupling. The analysis presented here is therefore somewhat uncertain. Nevertheless, it appears reasonably consistent with the experimental results.

The available input channels for formation of negative-ion resonant states are, using the notation introduced earlier, $^2S_{1/2}$, $^2P^0_{3/2,1/2}$, $^2D_{5/2,3/2}$, etc., corresponding to scattering states $4p^6\epsilon s$ $(J=\frac{1}{2})$, $4p^6\epsilon p$ $(J=\frac{3}{2},\frac{1}{2})$, etc. The lowest-lying negative-ion states expected to be formed belong to the configurations $4p^5 5s5p$ and $4p^5 5s4d$. A number of the many possible terms that can be formed in each of these configurations can be eliminated. J values greater than $\frac{5}{2}$ are unlikely since the low values of f-wave phase shifts in the energy range studied here imply that excitation via the $^2F_{7/2,5/2}$ channels is weak. Furthermore, the $4p^5 5s5p$ configuration is even parity so that resonances belonging to this configuration can only be found in the $^2S_{1/2}$, $^2D_{3/2}$, or $^2D_{5/2}$ incident channels, whereas $4p^5 5s4d$ configuration is odd parity and the only available channels for resonant formation (excluding the possi-

bility of f-wave formation) are $^2P^0_{3/2}$ and $^2P^0_{1/2}$.

The decay patterns of the $4p^5_{1/2}5s^2\,^2P_{1/2}$ resonance provide two clues as to why narrow resonances are observed at higher energies. First, the weak decay of the $^2P_{1/2}$ resonance to the $4p^5_{3/2}5s$ $J=2$ channel means that emission of electrons with $l \geq 2$ is unlikely in the decay process. Second, the fact that the $^2P_{1/2}$ resonance is narrow (<0.1 eV) even though decay into the $4p^5_{3/2}5s$ $J=1$ channel is possible implies that narrow resonances can occur provided the only possible decay modes involve participation of a $4p$ core electron.

The above facts make it seem likely that the narrow resonances in the 10.5–12.10-eV region are due to alternative levels of the $4p^55s4d$ configuration. Decay of resonances of the form $4p^5_{3/2}5s4d$ to the levels $4p^5_{3/2}5s$ $J=2, 1$ can only occur with emission of an $l=2$ electron unless the core participates in the decay process. Therefore, narrow resonances of this type may be expected at energies lower than 11.303 eV (the lowest $4p_{3/2}5p$ level) and analogously narrow resonances of the type $4p^5_{1/2}5s4d$ may be expected below 12.10 eV. On the other hand, states of the configurations $4p^5_{3/2,1/2}5s5p$ could decay directly with emission of an $l=1$ electron without core participation provided they lie above the lowest $4p^5_{3/2,1/2}5s$ levels (9.91 and 10.56 eV, respectively) and probably would be too broad to be detected.

Even with the restriction of possible $4p^55s4d$ resonances to the $^2P_{3/2}$ and $^2P_{1/2}$ input channels a number of resonances are possible. There will be four possible $^2P_{1/2}$ channel resonances (corresponding to ^2P, ^2D, ^4P, and ^4D $L-S$ coupling designations) and seven $^2P_{3/2}$ channel resonances (^2P, ^2P, ^2D, ^2D, ^4P, ^4D, and ^4F in $L-S$ coupling). While it appears likely that some if not all of the resonances below 12.10 eV are due to states of the $4p^55s4d$ configuration, it appears impossible from the available data to classify these levels further.

The interpretation of the narrow krypton resonances as $4p^55s4d$ levels appears to be supported by Beutler's classic work on the isoelectronic rubidium spectra.[24]

Beutler observed absorption of rubidium in the spectral range 600–900 Å and obtained a number of spectral lines corresponding to transitions of the type $4p^65s \rightarrow 4p^5_{3/2,1/2}5snl$. The strongest observed features correspond to transitions $4p^65s \rightarrow 4p^5_{3/2,1/2}5s^2\,^2P_{3/2,1/2}$ in analogy with the lowest krypton resonances. At shorter wavelengths a number of levels are observed the lowest of which Beutler ascribes to the $4p^55s4d$ configuration. Similar results have been obtained for Cs [25] and K,[26] elements with the same $np^6(n+1)s$ structure.

The energies of the Kr resonances appear related to those of the resonances observed in Rb by Beutler. This relationship is illustrated in Table II where the energies of levels in Rb belonging to the $4p^55s^2$ and $4p^55s4d$ configurations are compared with those of the krypton resonances. While no assignments can be made on the basis of this comparison it does indicate that the energy spread of the observed krypton negative ion resonances is approximately that expected of alternative levels of the $4p^55s4d$ configuration. The observed resonances above the first excitation threshold in Ne, Ar, and Xe [10] also appear to have spacings comparable to the spacings of np^5 $nd(n+1)s$ configurations in Na,[27] K [26] and Cs,[25] respectively. Further analysis of the negative ion resonance structures could be made by computation of the energy levels of $np^5nd(n+1)s$ configurations using theoretical level parameters as has been done for potassium.[28]

Although the sharp resonance peaks are the most striking feature of the excitation functions they make up a small fraction of the total intensity. Broad resonance features are present in some of the excitation curves presented, whereas others show a sharp rise at threshold followed by either almost constant excitation or a decrease in intensity. Sharp resonances are present at energies higher than 12.0 eV particularly in the curves for states of higher excitation.

It appears almost impossible to characterize the general behavior of the excitation functions at higher energies in terms of individual resonances.

TABLE II. Comparison of the energies of Rb I (Ref. 24) levels observed in absorption with the energies of negative ion resonances in Kr. All levels classified as belonging to the $4p^55s^2$ and $4p^55s4d$ configuration of Rb I are included. The energies of the Rb I resonances above the $4p^65s$ ground state have been arbitrarily scaled by 0.622 for comparison with the energies of the negative-ion resonances.

Resonance	Energy (eV)	Scaled energy	Neg. ion resonances
$4p^5_{3/2}5s^2$	15.31	9.52	9.52
$4p^5_{1/2}5s^2$	16.16	10.04	10.14
$4p^5_{3/2}(5s4d)$	17.21	10.69	10.67
$4p^5_{3/2}(5s4d)$	17.35	10.78	
$4p^5_{3/2}(5s4d)$	18.04	11.21	11.29
$4p^5_{3/2}(5s4d)$	18.11	11.25	11.42
$4p^5_{3/2}(5s4d)$	18.20	11.31	
$4p^5_{3/2}(5s4d)$	18.27	11.35	
$4p^5_{1/2}(5s4d)$	18.29	11.36	11.67
$4p^5_{3/2}(5s4d)$	18.46	11.48	
$4p^5_{1/2}(5s4d)$	18.93	11.76	11.97
$4p^5_{1/2}(5s4d)$	19.10	11.87	12.04
$4p^5_{1/2}(5s4d)$	19.13	11.88	12.10
$4p^5_{1/2}(5s4d)$	19.21	11.94	

However, the data do provide some information on the lowest broad features apparent in $4p^5 5s$ excitation. A broad feature appears at ≈11.1 eV in $4p^5_{3/2}5s$ $J=2$ and $J=1$ excitation. The over-all shape of the excitation curves for these two states is quite similar. The $4p^5_{1/2}5s$ $J=1$ excitation curve shows a similar broad structure at ≈11.8 eV, which is not present in the $4p^5_{1/2}5s$ $J=0$ excitation curve. These features are probably $^2D_{3/2}$ or $^2D_{5/2}$ resonances, the lower resonance formed from the $4p^5_{3/2}$ core and the upper from the $4p^5_{1/2}$ core. (Note that a $^2D_{5/2}$ resonance cannot decay to the $4p^5_{1/2}5s$ $J=0$ level with emission of an $l=1$ electron.) The existence of broad resonance structure in the $4p^5_{3/2}5s$ excitation curves is consistent with the rather sharp threshold behavior of the $4p^5_{3/2}5p$ excitation functions. Peaks occur near threshold in the $4p^5_{3/2}5p$ $J=1$ (11.30) and $J=1, 2$ (11.54) excitation functions due to the sharp resonances at 11.42 and 11.67 eV but part of the peak intensity may be due to broad resonances lying below the thresholds.

VI. SUMMARY AND CONCLUSIONS

The work reported here is more of an exploratory effort to provide information on resonant effects near excitation thresholds than an attempt to provide definitive data on individual excitation processes. The major results of our study are as follows.

(i) The classification of the lowest two resonances as $4p^5_{3/2,\,1/2}5s^2\,^2P_{3/2,1/2}$ is supported by our analysis.

(ii) There are both sharp and broad resonance features in near-threshold excitation in krypton. Some of the sharp features may be ascribed to individual resonances but some may be due to the effects of the opening of new channels for excitation. The broad resonant structure cannot be ascribed to any individual resonant states at present but appears to be responsible for a major part of the near-threshold excitation.

(iii) The sharp resonances in the 10.5–12-eV range observed both in our measurements and in transmission[10] appear to be $^2P_{3/2}$ or $^2P_{1/2}$ resonances with a $4p^5 5s4d$ configuration. If this interpretation is correct, sharp resonances of this type should be present in other atoms as well. The sharp resonances lying in the near-threshold region observed in transmission in other rare gases[10] may be of this type.

(iv) If the interpretations given here are correct there seems to be (for krypton at least) a tendency for negative ion resonances to decay only with emission of electrons with angular momentum quantum numbers $l=0$ or 1. If this tendency is true generally it would greatly facilitate the analysis of resonance structure from measurements made at several different angles of scattering. Further work, both theoretical and experimental, is needed.

(v) One of the most striking features of our study is the marked difference in both shape and intensity of excitation curves for levels separated by only a few tenths of an electron volt. The general picture that emerges is that resonant effects produce markedly different effects upon the excitation of different levels belonging to the same atomic configuration. Further theoretical and experimental work is needed in order to determine whether any general rules or relationships can be formulated.

ACKNOWLEDGMENT

The authors would like to thank Dr. D. L. Ederer for providing the resonance fits to the experimental data on elastic scattering.

APPENDIX

Expressions for the resonant and nonresonant parts of the scattering amplitudes f and g of Eq. (3) are given in Eqs. (4) and (5). Each of these amplitudes can be cast in the form

$$f, g = A + B\exp(-2i\cot^{-1}\epsilon), \tag{A1}$$

where A and B are complex quantities which depend only on the background phase shifts and the Legendre functions $P_l^m(\cos\theta)$ $(m=0, 1)$. Each component of the differential scattering is then given as

$$\begin{aligned}|f|^2,\ |g|^2 &= |A|^2 + |B|^2 + AB^*\exp(2i\cot^{-1}\epsilon) \\ &\quad + A^*B\exp(-2i\cot^{-1}\epsilon) \\ &= |A|^2 + |B|^2 + AB^*\frac{1+i\epsilon}{1-i\epsilon} + A^*B\frac{1-i\epsilon}{1+i\epsilon} \\ &= |A|^2 + |B|^2 \\ &\quad + \frac{(AB^* + A^*B)(1-\epsilon^2) + 2i(AB^* - A^*B)\epsilon}{1+\epsilon^2}.\end{aligned} \tag{A2}$$

The coefficients in Eq. (A2) are all real quantities and the expression can be written

$$|f|^2,\ |g|^2 = \alpha + \frac{\beta(1-\epsilon^2) + \gamma\epsilon}{1+\epsilon^2} \tag{A3}$$

and $|f|^2 + |g|^2$ is obviously of the same form and can be cast in the resonant form of Eq. (6). A comparison of Eq. (A3) with Eq. (6) yields the following relations:

$$(q^2-1)/q = 4\beta/\gamma\,, \tag{A4a}$$

$$\sigma_a = 2\beta/(q^2-1)\,, \tag{A4b}$$

$$\sigma_b = \alpha - \beta - \sigma_a\,, \tag{A4c}$$

$$\rho^2 = \frac{\sigma_a}{\sigma_a+\sigma_b} = \frac{2\beta}{(q^2-1)(\alpha-\beta)}\,, \tag{A4d}$$

which make it possible to obtain q and ρ from the quantities α, β, and γ.

---

[1]An excellent review has recently been completed by G. J. Schulz [Rev. Mod. Phys. 45, 378 (1973)].

[2]J. W. McGowan, J. F. Williams, and E. K. Curley, Phys. Rev. 180, 132 (1969).

[3]W. R. Ott, W. Kauppila, and W. L. Fite, Phys. Rev. A 1, 1089 (1970).

[4]G. E. Chamberlain, Phys. Rev. 155, 45 (1967).

[5]H. Ehrhardt, L. Langhans, and F. Linder, Z. Phys. 214, 179 (1968).

[6]P. G. Burke, S. Ormonde, and N. Whittaker, Proc. Phys. Soc. Lond. 92, 319 (1967).

[7]P. G. Burke, A. J. Taylor, and S. Ormonde, Proc. Phys. Soc. Lond. 92, 345 (1967).

[8]P. G. Burke, J. W. Cooper, and S. Ormonde, Phys. Rev. 183, 245 (1969).

[9]F. M. J. Pichanick and J. A. Simpson, Phys. Rev. 168, 64 (1963).

[10]L. Sanche and G. J. Schulz, Phys. Rev. A 5, 1676 (1972).

[11]D. Andrick, M. Eyb, and M. Hoffman, J. Phys. B 5, 215 (1972).

[12]G. J. Schulz, Phys. Rev. 116, 1141 (1959).

[13]R. H. Compton, R. H. Huebner, P. W. Reinhardt, and L. G. Christophorou, J. Chem. Phys. 48, 901 (1968).

[14]A summary of work of this type is contained in a paper by B. L. Moiseiwitsch and S. J. Smith, Rev. Mod. Phys. 40, 238 (1968).

[15]C. E. Kuyatt, J. Arol Simpson, and S. R. Mielczarek, Phys. Rev. 138, A385 (1965).

[16]D. Andrick and H. Ehrhardt, Z. Phys. 192, 99 (1966).

[17]N. F. Mott and H. S. W. Massey *The Theory of Atomic Collisions*, 3rd ed. (Oxford U. P., Oxford, 1965), p. 228ff.

[18]J. Holtzmark, Z. Phys. 66, 49 (1930).

[19]U. Fano and J. W. Cooper, Rev. Mod. Phys. 40, 441 (1968), especially p. 495, Eq. (8.5).

[20]See D. L. Ederer [Appl. Opt. 8, 2315 (1969)] for further details of the procedure.

[21]N. Swanson, J. W. Cooper, and C. E. Kuyatt, in *Proceedings of the Seventh International Conference on the Physics of Electronic and Atomic Collisions*, edited by J. B. Hasted (North-Holland, Amsterdam, 1972), p. 323.

[22]Effects of this type are usually discussed in terms of a two-channel case (elastic scattering and one inelastic channel) with the further assumption that only states of zero angular momentum of the scattering system make appreciable contributions to the near-threshold inelastic scattering (see, e.g., Ref. 17, p. 379ff). However, the theoretical arguments (which are based on the unitarity of S matrices describing the scattering process for definite values of total angular momentum and parity) upon which this effect is based also apply to pairs of inelastic channels and states of nonzero angular momentum. See, e.g., V. S. Baroshenkov [*Interaction Cross Section of Elementary Particles*, translated by Y. Oren (Israel Program for Scientific Translation, Jerusalem, 1968), Chap. X, p. 346ff] for a theoretical discussion of this point. The effect here is probably due to enhancement of excitation of the $4p\,^5_{3/2}\,5s\;J=1$ state in the $^2P_{1/2}$ channel at threshold due to the resonance lying immediately above threshold. It should be noted that effects of this type may be responsible for some of the sharp features appearing in the excitation curves presented in this paper occurring near higher thresholds of excitation.

[23]The analysis presented here follows closely that outlined by U. Fano and J. W. Cooper [Phys. Rev. 138, A400 (1965)].

[24]H. Beutler, Z. Phys. 91, 131 (1934).

[25]H. Beutler and K. Guggenheimer, Z. Phys. 88, 25 (1934).

[26]R. D. Hudson and V. L. Carter, J. Opt. Soc. Am. 57, 1471 (1967).

[27]T. Lucatorto and D. L. Ederer (private communication).

[28]W. C. Martin, J. L. Tech, and M. Wilson, Phys. Rev. 181, 66 (1969).